Amazonian Mesoscale Convective Systems: Life Cycle and Propagation Characteristics

Evandro M. Anselmo[1,2] Luiz A. T. Machado[1,4], Courtney Schumacher[2] and George N. Kiladis[3]

1. **National Institute for Space Research, São José dos Campos, São Paulo, 12227-010, Brazil**
2. **Texas A&M University, College Station, Texas, 77843**
3. **Physical Sciences Laboratory, NOAA, Boulder, CO, 80305**
4. **Department of Multiphase Chemistry, Max Planck Institute for Chemistry, Mainz, 55128, Germany**

Keywords: Amazonia, Kelvin waves, life cycle, mesoscale convective systems tracking

Corresponding author contact details: Evandro M. Anselmo, National Institute for Space Research, Rodovia, Presidente Dutra, km 40, INPE/CPTEC, 12630-970, Cachoeira Paulista/SP Brazil. e-mail: edromzans@pm.me

Abstract

Convective system tracking was performed using 30-min GOES-13 infrared imagery over the Amazon region during 2014 and 2015. A total of 116,701 convective systems were identified and statistics on the probability of occurrence of track area, lifetime and system velocity were analyzed. Maps of the total and seasonal geographic density of trajectories and the geographic density of clusters at genesis, during propagation, and at dissipation were also assessed. The mean area and lifetime of the tracked systems was 4×10^4 km^2 and 3 hours, respectively. The top 10% largest systems had areas $> 8 \times 10^4$ km^2 and the top 10% longest lived systems lasted > 7 hr. The geographical distribution of clusters identified on the coast and within the Amazon basin varied seasonally and their life cycle tracking showed that they are typically distinct from one another (i.e., it is relatively rare for systems to start at the coast and propagate 1500 km to the center of the basin). Although the average system velocity indicated a predominantly westward motion, a large spread in the direction of propagation was found. In particular, the probability of a meridional component of motion was generally the same for northward or southward directions and 35% of the zonal propagation was associated with eastward movement. The presence of Kelvin waves accounted for some of the eastward system motion, in addition to increasing the area and lifetime of storms compared to when Kelvin waves were not present.

1. Introduction

The Amazon is one of the wettest regions on earth. Most of its rainfall is organized by mesoscale convective systems (Nesbitt 2006), which are in turn modulated by the background atmospheric conditions. Amazonian mesoscale convective systems (AMCSs) are defined in this study as a general descriptor of organized convective cloud clusters observed in the Amazon basin and neighboring regions, including the coast. AMCS propagation and evolution is complex and depends on several factors, such as the large-scale circulation, topography, and river and sea breezes (e.g., Oliveira and Fitzjarrald, 1993; Cohen et al., 1995; Anselmo et al., 2020). For example, satellite studies generally report a predominantly westward propagation of convective systems across the Amazon basin associated with the easterly trade winds (e.g., Machado et al., 1998; Rehbein et al., 2017). However, during the Wet Season Atmospheric Mesoscale Campaign/Large-Scale Biosphere-Atmosphere experiment (WETAMC/LBA; see Silva Dias et al., 2002 for a detailed description), Laurent et al. (2002) showed that convective systems can have nearly stationary propagation speeds or even travel eastward in the southwestern Amazon during a mid-level westerly wind regime. Angelis et al. (2004) also found rain band propagation from the Andes towards the central Amazon using radar observations from the Tropical Rainfall Measuring Mission (TRMM) satellite. They argued that orographically induced winds affected convective system propagation in many of those cases.

Greco et al. (1990) described three types of AMCS propagation during the Amazon Boundary-Layer Experiment (ABLE 2B). The first type includes coastal systems corresponding to large squall lines that form along the northern coast of Brazil and propagate westward across the Amazon basin. These systems were also described by Garstang et al. (1994) and named Amazon Coastal Squall Lines (ACSLs). ACSLs have been associated with large amounts of nighttime precipitation in the southwest and central Amazon (Rickenbach, 2004; Tang et al., 2016). The second type is basin occurring systems, which form in the central Amazon and propagate to the west. The third type corresponds to locally occurring systems, which have a short life cycle and minimal propagation.

The classification of convective systems as coastal, basin and locally occurring has in the past been based on visual inspection using geostationary imagery (Kousky, 1980; Greco

et al., 1990; Garstang et al., 1994; Cohen et al., 1995). Due to the large amount of convective clouds and the complex aggregation of cloud types in the Amazon basin, it is difficult to subjectively follow and describe in detail convective cloud system initiation, merging, splitting and dissipation. Tang et al. (2016) analyzed these three convective system types in the context of the Observation and Modeling of Green Ocean Amazon field campaign (GoAmazon2014/5; see Martin et al., 2016 for a detailed description) and point out that the differentiation between basin and coastal systems is difficult. Burleyson et al. (2016) postulated that some ACSLs could propagate from the coast and arrive in the Manaus region in the central Amazon the next day in phase with the local diurnal surface heating; however, differentiating between local and non-local convection is not trivial. Kelvin waves also impact MCS frequency and activity in Amazonas. Serra et al. (2020) demonstrated that the active phase of Kelvin waves modifies the local environment in the central Amazon, creating a deep layer of moisture that favors more organized convection.

This study employs an automatic tracking algorithm using GOES satellite images, similar to the tracking algorithms used by Woodley et al. (1980), Williams and Houze (1987), Chen et al. (1996), Machado et al. (1998), Mathon and Laurent (2001) and Vila et al. (2008), to evaluate convective system trajectories and evolution over the Amazon basin. The tracking technique is based not only on the convective system mass center, but also takes into account its total area. This adjusted tracking technique allows one to evaluate where systems originate (i.e., the coast or central basin) and subsequent merging, splitting and dissipation. Machado et al. (2018) combined radar and satellite data to study convective system and rain cells during the GoAmazon field campaign. They found that the typical AMCS has a 75-km effective radius and 1.5 hours lifetime, while rain cells are 10 times smaller and have a typical lifetime of 0.6 hours.

The main goal of this study is to present an objective description of the seasonal variation of the spatial distribution and life cycle characteristics of AMCS trajectories over the Amazon basin. This study describes the density of convective systems during three lifetime stages: initiation, mature and dissipation. In addition, a separate analysis is performed for the systems reaching the central Amazon. This study also provides a climatology describing the pattern and variability of the AMCS speed, probability of

occurrence and propagation direction as well as a discussion of Kelvin wave effects on AMCSs.

2. Methodology

2.1 Cloud cluster tracking

GOES-13 channel 4 (10.2-11.2 μm) infrared imagery was used to track AMCSs during 2014 and 2015, the two years of the GoAmazon2014/5 experiment. The GOES imagery is stored by the National Institute for Space Research (INPE) every 30 min with 4 km × 4 km spatial resolution at nadir. Occasionally, higher frequency images (every 15 minutes) were also available and employed in this study. The analyzed region (15°S-13°N, 82°-34°W) covers the entire Amazon basin.

Regions with a continuous cloud area greater than or equal to 2400 km^2 and cloud top brightness temperature (Tb) less than or equal to 235 K were defined as cloud clusters. These thresholds were previously employed in several studies over the Amazon (e.g., Machado et al., 2002). Cloud clusters in successive images were compiled to define the full life cycle of each convective system. There are occasional time gaps in the satellite imagery and the maximum time tolerance after which tracking was stopped was one hour (i.e., the algorithm did not continue to track systems if there were more than two missing 30-min observations). During the two years analyzed, among the 30,474 images evaluated, there were four time gaps with more than one day (from 1 day to 4 days in one case), 576 gaps of 3 hours, 71 gaps of 2.5 hours, 38 gaps of 2 hours, and 76 gaps of 1.5 hour.

The minimum overlap to identify cloud clusters in two successive images was fixed at 150 pixels, roughly corresponding to a cloud cluster with a radius of 27 km. This value was chosen based on Vila et al. (2008) who, after considering a convective system as an elliptical shape with 0.5 eccentricity and an average speed of 45 km/h, concluded that an overlap larger than 150 pixels is most appropriate for the time step of 30 minutes and spatial resolution of 4 km × 4 km at nadir, the same employed in this study.

Tracking can reveal pathways that connect clusters in time and space between an image at t_0 and an image at $t_0 + dt$. The possible pathways are described by Vila et al. (2008)

as: continuity, merge, and split. Woodley et al. (1980), Williams and Houze (1987) and Mathon and Laurent (2001) also discuss these possibilities in cloud cluster tracking using satellites. Continuity is the condition when there is only one overlapping between a cluster at t_0 and t_0 + dt. Merger is the condition when there are two or more clusters at t_0 overlapping with a cluster at t_0 + dt. Finally, split is the condition when a cluster at t_0 overlaps with two or more clusters at t_0 + dt.

Figure 1 presents an example of possible multiple processes in cloud cluster connections. Cluster 4 at t_0 + dt could result from a merger between clusters 3 and 6 at t_0. Clusters 2, 4, and 5 at t_0 + dt may be a result of a split from cluster 3 at t_0, while cluster 2 at t_0 + dt could be formed from a merger between clusters 1 and 3 at t_0. Considering the maximum overlap between clusters (Mathon and Laurent, 2001), we are fairly certain that cluster 1 is connected with cluster 2 and that cluster 3 is connected with cluster 4, i.e., there are only two solutions when considering the maximum area overlap.

The tracking algorithm can provide information on whether the cloud cluster genesis is a result of a new cluster initiation or if it was initiated by a split from another cluster. In addition, dissipation can be evaluated as due to cloud decay or as a merger into another system (the larger overlapping cluster continues to be tracked and the other is considered dissipated by merge). Additionally, continuity, merger, and split pathways can occur simultaneously (Woodley et al., 1980; Mathon and Laurent, 2001).

Based on the two-year data set and 235 K threshold, there were 668,894 cluster overlaps to evaluate. Simple continuity, i.e., without any split-merger, represented 83.4% (558,082) of the cases, mergers represented 5.4% (35,826), splits represented 5.6% (37,578), and multiple processes represented 5.6% (37,408). Inside of the 37,408 instances of cluster overlap associated with multiple processes, there were 73,222 valid connections between clusters at t_0 and t_0 + dt, i.e., 10% of the total pathways of connections. Machado and Laurent (2004) only selected convective systems with spontaneous initiation and dissipation because they were looking for area expansions of clusters and their lifecycles. The tracking algorithm in this study selects cloud clusters independent of the type of initiation or dissipation, since the main goal is evaluating the trajectories.

The tracking process provides information about the AMCS lifetime, displacement,

velocity and the bidimensional trajectory (the area trajectory). In previous studies, such as Aspliden et al. (1976), Martin and Schreiner (1981), Machado et al. (1998) and Sakamoto et al. (2011), the trajectories of the systems were represented with a line connecting the geometrical center or weighted centroid of each cloud cluster that defined the system. In this study, the trajectory is not considered in such a linear fashion. Here, the trajectory represents the union of all pixels (the total cloud cluster area) that define the AMCS. Figure 2 presents an example of the trajectory of an AMCS tracked on 21 March 2014; the trajectory is the gray area in the image and the colors are the brightness temperature.

2.2 Kelvin wave dataset

TRMM 3B42 precipitation anomalies were computed for 2014 and 2015 and a Kelvin wave filter was applied based on the Wheeler and Kiladis (1999) space-time filter. Using the cluster tracking statistics composited with respect to Kelvin wave precipitation anomalies, we examined how Kelvin waves may affect the life cycle and propagation of convective systems across the Amazon. Regions with a filtered Kelvin wave precipitation anomaly > 0.1 mm/h were considered to be within a positive Kelvin wave phase, while regions with a filtered Kelvin wave precipitation anomaly < -0.1 mm/h were considered to be a negative Kelvin wave phase. To evaluate the relationship between Kelvin waves and AMCSs, the following criteria were employed:

- AMCS initiation under the influence of a positive (negative) Kelvin wave phase requires at least 95% of the cloud cluster area, during the initiation, to be over the positive (negative) Kelvin wave phase region.
- AMCSs under the influence of a positive (negative) Kelvin wave phase need to have at least 70% of the cloud cluster area, during their life cycle, overlapping with a positive (negative) Kelvin wave phase region.

With this dataset combination, it was possible to assess the potential Kelvin wave impact on AMCS initiation, trajectories and lifetime.

3. Results

3.1 Convective system area and lifetime distributions

The tracking algorithm identified 116,701 convective systems that were connected in at least two consecutive satellite images. Figure 3 presents the probability distribution function (PDF) and the cumulative distribution function (CDF) of cloud cluster track areas and lifetimes. The track areas and lifetimes were binned by 2500 km^2 and 0.5 h, respectively. The mean size and lifetime of the AMCSs were 4.1×10^4 km^2 and 3.1 h. The median track area (or 50th percentile of the CDF) was 1.5×10^4 km^2, the 90th percentile area was 7.7×10^4 km^2, and the maximum area was 5.3×10^6 km^2. The lifetime PDF decreases exponentially, with a median lifetime of 1.5 h. For the 90th percentile, lifetime was 7 h; however, the longest-lived system lasted 82 h. These results agree with the average convective system size and lifetime obtained by Machado et al. (2018) during the Amazon wet and dry season.

3.2 Geographic patterns of convective system occurrence

AMCS occurrence was computed on a 0.04° × 0.04° resolution grid to assess their spatial distribution across the Amazon basin. The frequency of occurrence was calculated by using the area covered by the convective cloud clusters and density values represent the number of systems crossing a grid normalized by the total number of convective systems tracked during the two-year period, expressed as a percentage. Figure 4a presents the spatial distribution of the AMCS density of occurrence and can be interpreted as the probability path of convective systems. Figure 4b presents the rain rate computed by the 1° TAPEER-BRAIN product (Roca et al., 2010; Chambon et al., 2012; Chambon et al., 2013) for the same period. TAPEER-BRAIN is the rainfall estimation produced from the Megha-Tropiques satellite that combines microwave and infrared observations (REFERENCE). While many satellite rainfall products are available for analysis, TAPEER-BRAIN compares favorably to other satellite rain retrievals over rainy land regions (e.g., Gosset et al. 2018) and was employed to simply show the qualitative relationship between AMCS occurrence and the rainfall pattern over the Amazon. As expected, the geographic density of trajectories agrees well with the daily accumulated surface rainfall, with the highest density of convective system occurrence associated with the largest rain amounts. This result shows that much of the precipitation in

the Amazon is from organized convective systems, consistent with Nesbitt et al. (2006).

Figure 4a shows that the maximum probability of convective system occurrence is over Colombia in the extreme northern part of the Andes. This region is convectively active throughout the year as discussed by Horel et al. (1989), Machado et al. (2004), Houze et al. (2015), Zuluaga and Houze (2015), Rasmussen et al. (2016) and Poveda et al. (2020). The next highest probability of convective system occurrence is across the central Amazon, presumably due to daytime heating, instability and the vertical distribution of water vapor (Schiro et al. 2016, Lintner et al. 2017) over the rainforest that promotes relatively frequent large diurnal convective systems. There is a third, small region of high AMCS probability along the Brazilian coast near the mouth of the Amazon river; however, Brazilian coastal regions further north and along the coasts of French Guiana, Suriname and Guyana have much smaller probabilities. Near the mouth of the Amazon river, the sea breeze and trade winds are nearly in the same direction. Northward along the coast, the sea breeze becomes nearly perpendicular to the trade winds, which may hinder convective system growth and propagation inland (Cohen et al., 1995). Topographic blocking also likely plays a role in this minimum.

There is a slight suppression of convection over the major rivers in the Amazon basin and the relative maxima in occurrence between these rivers is probably related to the river breeze circulation triggering convection as discussed Santos et al. (2014). There is a sharp drop in the probability of occurrence between the coast and central Amazon to the northeast of a northwest-southeast line from 7° S, 48° W and 3° N, 68° W. This is an important feature to note since it suggests that AMCSs do not typically travel from the coast straight into the central Amazon. This feature will be discussed in detail in the next section.

The seasonal influence on AMCS density can be seen in Figure 5. The densities for December, January, February (DJF); March, April, May (MAM); June, July, August (JJA); and September, October, November (SON) were gridded separately and the geographic probability density in each season is shown as a percentage as in Figure 4a. In general, the density of AMCS occurrence inside the studied region follows the path of the sun with maximum probabilities concentrated in the south during DJF (Figure 5a) and in the north

during JJA (Figure 5c). However, there is also a zonal shift with MAM being the dominant season for coastal systems (Figure 5b) and SON being dominated by systems in the western Amazon basin with very little coastal convection (Figure 5d), consistent with Greco et al. (1990). MAM presents the highest AMCS probability on the coast and is also the season where more ACSLs propagate into the central Amazon (Cohen et al., 1995; Alcântara et al., 2011). In DJF, the AMCS density is higher in Central Amazonas and over the Andes in the southwest of the region, however, over the coast it has a smaller probability than during MAM, so fewer coastal systems exist to propagate westward to the central Amazon.

3.3 Convective system life cycle

In order to describe the evolution of AMCSs, the geographical distribution of occurrence was computed for different stages of the AMCS lifecycle. To focus on the spatial distribution of long-lived AMCSs, systems lasting more than 2.5 hours were selected to guarantee at least five 30-min time steps, which resulted in a total of 42,527 systems. Each system was classified into five stages: the initiation (t_i) and dissipation (t_f) stages and three intermediary stages numbered 1, 2 and 3 representing the propagation of the system between genesis and dissipation (i.e., t_1, t_2, and t_3). The average lifetime of this sample is 6.4 hours, corresponding to t_i the first time the system was detected, t2, t3 and t4 at 1.6, 3.5 and 4.8 hours later and t_f 6.4 hours later. While there is geographical variability in cloud cluster occurrence by season (Figure 5), the relative patterns of genesis and dissipation do not change considerably by season (not shown). Thus, we focus on analysis of the annually averaged data.

Figure 6 shows the gridded cloud cluster spatial distribution for each normalized time step. The probability values represent area percentages in each $0.04° \times 0.04°$ grid box based on the 42,527 systems. In general, there is an expansion of cluster area from genesis until t_2, when most of the convective systems reach maturity. After that, a decrease of cluster area occurs until dissipation. Because systems are smaller during initiation and dissipation, the probability is smaller since the entire storm area is considered, not just the AMCS mass center. Thus, the larger the system, the more grid boxes are counted in the statistics.

Figure 6a shows that the main initiation region of coastal AMCSs is near the mouth

of the Amazon River. AMCS initiation also occurs over a much larger region across the central Amazon and in the higher topography region in the northwest Amazon. In the following time step (t_1), AMCSs expand across the central and northwest Amazon (Fig. 6b). They also cover a larger area of the coast, but with a higher probability south of the Amazon River compared to the north. At t_2, the central Amazon systems expand westward and the coastal systems show distinct inland propagation (Fig. 6c). However, a line of low probability oriented northwest southeast separates the AMCSs that form and grow on the coast from the AMCSs that form and grow in the central Amazon. This line is parallel to and 500-1000 km from the coast. This break in AMCS cloud cover evolution suggests that the AMCSs that form on the coast are distinct from the AMCSs that form in the central and northwest Amazon. The break is also consistent with the minimum in rainfall seen in Fig. 4b. At t_3, just before dissipation, the systems that initiated on the coast are furthest from the coast while the central Amazon systems tend to be decaying in place (Fig. 6d). At the dissipation stage (t_f), systems are smaller and the probabilities are reduced across northern South America (Fig. 6e). The remaining signal close to coast likely represents ACSLs that were short lived, classified by Greco et al. (1990) as coastal systems. Over the Andes, in the southwest of the study region, there are some spots of high probability of AMCS occurrence, but with a nearly constant position in different phases, corresponding to slight propagation.

The rainfall in central and southwest Amazon exhibits frequent nocturnal and early morning precipitation events (Machado et al., 2002; Machado et al., 2004; Rickenbach, 2004). This nocturnal secondary maximum in the diurnal cycle has been attributed to mesoscale convective activity propagating from the east associated with ACSLs (Garstang et al., 1994). Nevertheless, when objectively following the tracked cloud clusters, very few AMCSs continually travel from the coast to the central Amazon. During the night, there appears to be a deintensification in convective activity and, in general, very little cold cloud shield is observed.

Based on visual examination of satellite image loops, around noon on the day after the AMCS deintensification, there is reactivation of the mesoscale convection hundreds of kilometers ahead of where the AMCS dissipated the night before. The trigger mechanism of this reactivation is still unknown. Anselmo et al. (2020) discuss the impact of the nocturnal

Amazonian low-level jet (ALLJ) on the propagation and life cycle of convective systems from the northeast coast of South America into central Amazonia. The ALLJ can act in different ways to produce the observed break and reactivation of the convection, as for instance by advection of humidity from the coast overnight that assists daytime convection the next day or by association with internal gravity waves that can propagate as described by Sun and Orlanski (1981). The reactivation could simply occur because of advection by the large-scale flow of a moisture tongue at mid-levels formed by the cloud shield dissipation from the day before. The reason of this reactivation is not the goal of this study and would certainly be worthy of a future study.

In order to check where the AMCSs that impact the central Amazon form, the following methodology was applied. All AMCSs lasting longer than 4 hours that crossed a 200-km radius around Manaus (located at 03° S, 60° W) were selected from the tracking database. Figure 7 shows the spatial distribution of the track density at the time of initiation of the 1396 selected AMCSs and the circle represents the 200-km radius. Only long-lived (> 4 hr) cloud clusters were analyzed to preclude local, short-lived convection that initiates around the search region. The spatial distribution reveals a wide diversity of initiation locations of long-lived convective systems within the vicinity of Manaus. However, it is clear that the dominant AMCS track affecting the Manaus region is not from the coast; the majority formed in the central Amazon.

3.4 Convective system propagation velocities

For each step in a convective system's life cycle, it is possible to determine the velocity of propagation. For the 116,701 convective systems identified during 2014 and 2015, 704,708 system velocities were computed. Velocity was calculated as the ratio between the distance of the geometric center at t_0 and t_0 + dt and the time interval between the successive satellite images.

Figure 8 presents the PDF and CDF of convective system velocities binned by 0.5 m/s of the zonal and meridional wind components (u and v), as well as the absolute velocity. The highest probability of u (2.9%) was -2.8 m/s (westward propagation) and the highest probability of v (4.0%) was 0.3 m/s (slight northward propagation). However, the distribution

of positive (eastward and northward propagation) and negative (westward and southward propagation) values show a large and generally symmetric spread about these median values, meaning that convective systems traveled across a large range of directions. For example, despite the predominantly westward propagation driven by the equatorial trade winds, 35% of the convective system zonal velocities had eastward propagation. Convective system meridional propagation has velocities roughly equally distributed between northward and southward, although this is more intuitive since the ITCZ shifts with the seasons causing the trade winds to have alternately northerly and southerly components throughout the year. The AMCS average speed of propagation was 12.9 m/s, the median (50th percentile of the CDF) was 7.9 m/s. The distribution shows outlier speeds larger than 20 m/s, probably related to a change in AMCS geometry from merging/splitting that could create a considerable change in a system's geometric center.

In order to provide the geographical distribution of AMCS propagation direction and speed, cloud cluster velocities were computed regionally and presented in the form of wind roses (Figure 9). More specifically, the wind roses presented in Figures 9 and 12 highlight the AMCS direction of propagation. Large westward propagation velocities occur over the Atlantic Ocean and along the east coast of South America. AMCS motion near the coast is probably associated with the ITCZ and ACSLs. Westward propagation is also dominant over the central Amazon. The northwestward and southwestward components of velocity over the central Amazon exhibit a nearly symmetric distribution, with a slight skew toward northwestward propagation. The northeastward, eastward and southeastward AMCS propagation velocities can be seen in all analyzed regions; however, they comprise only approximately 30% of all systems. The propagation near the Andes is less organized, sometimes without a dominant direction of propagation. Also, in the southeast of the analyzed region one can note a predominant eastward propagation, possibly associated with cold fronts propagating toward the Atlantic Ocean.

In general, four propagation regimes can be identified in Figure 9, the first one over the Atlantic Ocean, where westward propagation is most dominant in the ITCZ region. The second one lies over the central Amazon, where westward propagation is also dominant but the spread in the direction of propagation is larger as we move toward that region. Over the

higher topography elevations near the Andes and in the northwest regions near the coasts, in general, there is no preferential direction of propagation. Finally, the fourth regime is in the south of the domain, where mid-latitude systems also penetrate into the region and there is no clear pattern. Over the four regimes of propagation, the maximum speed of propagation is associated with westward motion, except for the southeastern-most domain, where eastward propagation displays the highest speeds.

3.5 Kelvin wave influence on convective system evolution and propagation

Evidence of convectively coupled equatorial wave propagation has been found through global satellite observations (Tanaka and Ryuguji, 1971; Wallace and Chang, 1972; Gruber, 1974; Zangvil, 1975; Takayabu, 1994; Kiladis et al., 2009) and these modes are associated with Matsuno's (1966) wave solutions of the shallow water equations. Here we analyze the convectively coupled Kelvin wave mode as isolated by the Wheeler and Kiladis (1999) space-time spectral filter to potentially explain part of the AMCS lifecycle and propagation variability over the Amazon.

Kelvin waves occur most often over northern South America in austral summer, specifically over the Amazon (Liebmann et al., 2009; Guo et al., 2014). Figure 10 provides an example of how often Kelvin waves cross equatorial South America from the central Pacific into the Atlantic and the precipitation anomaly associated with their passage. During this period (January-March 2014), Kelvin wave activity maximizes near the longitude of Manaus (indicated by the vertical line).

During the full two-year period and among the 116,701 total initiations reported in this study, genesis occurred 15,538 times during a positive Kelvin precipitation anomaly (i.e., > 0.1 mm/h), which corresponds to about 13% of the total events. When Kelvin wave precipitation anomalies were negative (< -0.1 mm/h), only 10,972 instances of genesis were detected, corresponding roughly to 9% of the AMCS initiations. Thus, AMCSs appear to have a marked preference for genesis during the convectively active phase of the Kelvin wave. The genesis in the positive phase shows an almost 50% increase in relation to the negative phase. However, one can also conclude that Kelvin waves are not the only factor in determining the genesis of AMCSs due to the large numbers of initiations not associated with

Kelvin waves.

When the complete set of AMCS trajectories are considered and not only the initiation phase, there are 18,747 systems tracked in the positive phase and 12,743 systems tracked in the negative phase. Figure 11 shows the relationship between AMCS area and lifetime distributions during both phases. AMCSs during positive Kelvin phases tend to be larger and longer lived, and the longest lived systems (i.e., those that last more than 10 hours) predominantly occur during the positive Kelvin wave phase. The very largest ($> 6.5 \times 10^5$ km^2) and longest lasting (> 30 hours) convective systems (representing the top 1% of the area and lifetime distributions) only occur during the positive Kelvin wave phase. A function fit in Figure 11 illustrates the different behavior of AMCSs during the two Kelvin wave phases. The larger power coefficient of the adjusted function during positive anomalies shows that AMCS area grows faster (i.e., a higher area expansion) during the passage of the convectively active portion of a Kelvin wave.

As discussed in section 3.4, about one third of the AMCSs have a component of eastward propagation across the Amazon, which is not intuitive in a regime dominated by strong easterlies. In order to evaluate if Kelvin waves are responsible for this anomalous propagation, we computed the AMCS propagation wind roses for only the positive Kelvin wave anomalies. We selected all cloud clusters at t_0 + dt with an eastward displacement that had at least 70% of its area inside the Kelvin wave region. We found 39,805 eastward steps during Kelvin wave passages, about 16% of the total times of eastward propagation. Figure 12 shows a wind rose plot similar to Figure 9, but only for systems that occur during positive Kelvin wave conditions. The strongest eastward propagation is seen over the Atlantic Ocean and along the east coast. There is generally a decrease in westward propagation over the central Amazon compared to Figure 9, while the convective systems near the Andes maintain a strong westward propagation component. The Kelvin waves seem to primarily modulate AMCS propagation over the ocean and coast, while over the Amazon they modulate the cloud cover area and system lifetime.

4. Conclusions

A climatology of AMCS area trajectories is presented for the tropical South America region based on cloud cluster tracking using two years of satellite images. High-resolution maps of the AMCS trajectories provide new details about the spatial distribution of AMCS occurrence as well as their genesis, propagation and dissipation. In addition, previous studies that tracked convective systems over the Amazon selected just those systems with simple initiation and dissipation, i.e., without merges and splits, but in this study all systems are tracked and analyzed.

Overall 116,701 systems were identified and the top 10% of trajectories and lifetimes, i.e., the long-lived systems, had areas greater than 8×10^4 km^2 and lifetimes greater than 7 hours. Mean area and lifetime were about half of these values. The central Amazon exhibited a widespread, homogeneous pattern of high convective system genesis probabilities. Some higher genesis probabilities were also associated with higher topography and the river breeze throughout the Amazon basin. Along the coast, convective systems occurred more often near the mouth of the Amazon river compared to further north along the coast. The occurrence of coastal and basin convective systems also had a seasonal dependence. For example, during SON, convective systems mostly formed in the central part of the Amazon basin while during MAM, AMCSs occurred both along the coast and the central Amazon and trajectories were more connected between the two regions.

By studying only the tracks of convective systems that crossed the region around Manaus in the GoAmazon2014/5 region, we found 1396 systems lasting longer than 4 hours and very few of these systems were initiated on the coast. During the two years studied, only 12 of these AMCSs were observed to do so. Most coastal AMCSs dissipate before the central Amazon, creating a region with fewer AMCSs and less rainfall. This region is nearly parallel to the coast and clearly shows the maximum distance that most ACSLs can propagate inland. In the central Amazon, there is a broad region of AMCS initiation. The hypothesis involving the propagation of a moisture tongue of humidity in the middle levels, formed by the dissipation of AMCS the day before, should be evaluated as a mechanism that assists in this broad region of AMCS activity.

This study also provides statistical characteristics of the AMCS velocity and direction of propagation with further potential for it to be used in forecast applications in tropical South

America. Although previous studies indicate predominantly westward displacement for AMCSs, a large spread in the direction of propagation was observed. For instance, in the central Amazon, purely westward propagation corresponds to only about 15% of the overall propagation distribution, while the remaining propagation vectors were distributed in other sectors. Convective system velocities showed practically the same probability of having a northward or southward propagation component and 35% of the zonal velocities were associated with a component of eastward movement. Westward motion was especially enhanced near the coast, while convective system propagation in the Andes was less predominantly westward.

Kelvin wave events appear to have a substantial influence on AMCS initiation. In particular, the convectively active part of the Kelvin waves tends to be associated with AMCSs that have larger areas and longer lifetimes consistent with the Serra et al. (2020) results focusing on MCSs detected by the GoAmazon2014/5 radar. There is also an increase in eastward propagation during the positive phase of the Kelvin wave, especially near the coast, that may be associated with low-level westerly anomalies along the western flank of the Kelvin wave. Future analysis of the propagation direction and speed dependencies on the basic state would help further explain the observed spread of AMCS propagation across the Amazon.

Acknowledgments

The CAPES Foundation grant 99999.000481/2016-05 and DOE grant DE-SC0016245 for financial support and FAPESP grant 2015/14497-0. We would like to thank Dave Adams and the anonymous reviewers for their suggestions.

Data Access

The GOES-13 convective system tracking data set will be archived at the Texas A&M University OAKTrust Digital Repository (http://oaktrust.library.tamu.edu).

References

Alcântara, C. R., Dias, M. A. S., Souza, E. P. and Cohen, J. C. (2011). Verification of the role of the low level jets in Amazon squall lines, Atmospheric Research 100(1): 36–44.

Anselmo, E., Schumacher, C., and Machado, L. (2020). The Amazonian low-level jet and its connection to convective cloud propagation and evolution. Monthly Weather Review 148: 4083-4099.

Angelis, C. F., McGregor, G. R. and Kidd, C. (2004). A 3-year climatology of rainfall characteristics over tropical and subtropical South America based on Tropical Rainfall Measuring Mission precipitation radar data, International Journal of Climatology: A Journal of the Royal Meteorological Society 24(3): 385–399.

Aspliden, C. I., Y. Tourre, and J. B. Sabine, (1976). Some Climatological Aspects of West African Disturbance Lines During GATE, Mon. Wea. Rev., 104, 1029–1035, https://doi.org/10.1175/1520-0493(1976)104<1029:SCAOWA>2.0.CO;2.

Burleyson, C. D., Feng, Z., Hagos, S. M., Fast, J., Machado, L. A. and Martin, S. T. (2016). Spatial variability of the background diurnal cycle of deep convection around the GoAmazon2014/5 field campaign sites, Journal of Applied Meteorology and Climatology 55(7): 1579–1598.

Chambon, P., Jobard, I., Roca, R. and Viltard, N. (2013). An investigation of the error budget of tropical rainfall accumulation derived from merged passive microwave and infrared satellite measurements, Quarterly Journal of the Royal Meteorological Society 139(673): 879–893.

Chambon, P., Roca, R., Jobard, I. and Aublanc, J. (2012). The TAPEER-BRAIN product: Algorithm theoretical basis document, level 4, Megha-Tropiques Tech. Memo 4: 13.

Chen, S. S., Houze Jr, R. A. and Mapes, B. E. (1996). Multiscale variability of deep convection in realation to large-scale circulation in TOGA COARE, Journal of the Atmospheric Sciences 53(10): 1380–1409.

Cohen, J. C. P. (1989). An observational study of Amazon squall lines (in portuguese), Master's thesis, Institute for Space Research, Sao Jose dos Campos – Brazil.

Cohen, J. C., Silva Dias, M. A. and Nobre, C. A. (1995). Environmental conditions associated with Amazonian squall lines: A case study, Monthly Weather Review 123(11): 3163–3174.

Garreaud, R. and Wallace, J. M. (1997). The diurnal march of convective cloudiness over the Americas, Monthly Weather Review 125(12): 3157–3171.

Garstang, M., Massie Jr, H. L., Halverson, J., Greco, S. and Scala, J. (1994). Amazon coastal squall lines. Part I: Structure and kinematics, Monthly Weather Review 122(4): 608–622.

Greco, S., Swap, R., Garstang, M., Ulanski, S., Shipham, M., Harriss, R., Talbot, R., Andreae, M. and Artaxo, P. (1990). Rainfall and surface kinematic conditions over central Amazonia during ABLE 2B, Journal of Geophysical Research: Atmospheres 95(D10): 17001–17014.

Gosset, M., Alcoba, M., Roca, R., Cloche, S., and Guillaume, U. (2018). Evaluation of TAPEER daily estimates and other GPM-era products against dense gauge networks in West Africa, analysing ground reference uncertainty, Quarterly Journal of the Royal Meteorological Society 144: 255-269.

Gruber, A. (1974). The wavenumber-frequency spectra of satellite-measured brightness in the tropics, Journal of the Atmospheric Sciences 31(6): 1675–1680.

Guo, Y., X. Jiang, and D.E. Waliser, 2014: Modulation of the Convectively Coupled Kelvin Waves over South America and the Tropical Atlantic Ocean in Association with the Madden–Julian Oscillation. J. Atmos. Sci., 71, 1371–1388, https://doi.org/10.1175/JAS-D-13-0215.1

Lintner, B. R., D. K. Adams, K. A. Schiro, A. M. Stansfield, A. A. Amorim Rocha, and J. D. Neelin (2017), Relationships among climatological vertical moisture structure, column water vapor, and precipitation over the central Amazon in observations and CMIP5 models, Geophys. Res. Lett., 44, doi:10.1002/2016GL071923.

Martin, D. W., and A. J. Schreiner, (1981). Characteristics of West African and East Atlantic Cloud Clusters: A Survey from GATE, Mon. Wea. Rev., 109, 1671–1688, https://doi.org/10.1175/1520-0493(1981)109<1671:COWAAE>2.0.CO;2.

Horel, J. D., Hahmann, A. N. and Geisler, J. E. (1989). An investigation of the annual cycle of convective activity over the tropical Americas, Journal of Climate 2(11): 1388–1403.

Houze Jr, R. A. (1993). Cloud dynamics, 573 pp, Academic, San Diego, Calif.

Houze, R. A., Rasmussen, K. L., Zuluaga, M. D., and Brodzik, S. R. (2015). The variable nature of convection in the tropics and subtropics: A legacy of 16 years of the Tropical Rainfall Measuring Mission satellite, Rev. Geophys., 53, 994–1021, doi:10.1002/2015RG000488.

Kiladis, G. N., Wheeler, M. C., Haertel, P. T., Straub, K. H. and Roundy, P. E. (2009). Convectively coupled equatorial waves, Reviews of Geophysics 47(2).

Kousky, V. E. (1980). Diurnal rainfal0l variation in northeast Brazil, Monthly Weather Review 108(4): 488–498.

Laurent, H., Machado, L. A., Morales, C. A. and Durieux, L. (2002). Characteristics of the Amazonian mesoscale convective systems observed from satellite and radar during the WETAMC/LBA experiment, Journal of Geophysical Research: Atmospheres 107(D20).

Liebmann, B., G. N. Kiladis, L. M. V. Carvalho, C. Jones, C. S. Vera, I. Bladé, and D. Allured, 2009: Origin of convectively coupled Kelvin waves over South America. J. Climate, 22, 300-315.

Machado, L. A. T. and Laurent, H. (2004). The convective system area expansion over Amazonia and its relationships with convective system life duration and high-level wind divergence, Monthly Weather Review 132(3): 714–725.

Machado, L., Laurent, H., Dessay, N. and Miranda, I. (2004). Seasonal and diurnal variability of convection over the Amazonia: a comparison of different vegetation types and large scale forcing, Theoretical and Applied Climatology 78(1): 61–77.

Machado, L., Rossow, W., Guedes, R. and Walker, A. (1998). Life cycle variations of mesoscale convective systems over the Americas, Monthly Weather Review 126(6): 1630–1654.

Machado, L. A. T., Calheiros, A. J. P., Biscaro, T., Giangrande, S., Silva Dias, M. A. F., Cecchini, M. A., Albrecht, R., Andreae, M. O., Araujo, W. F., Artaxo, P., Borrmann, S., Braga, R., Burleyson, C., Eichholz, C. W., Fan, J., Feng, Z., Fisch, G. F., Jensen, M. P., Martin, S. T., Pöschl, U., Pöhlker, C., Pöhlker, M. L., Ribaud, J.-F., Rosenfeld, D., Saraiva, J. M. B., Schumacher, C., Thalman, R., Walter, D., and Wendisch, M. (2018). Overview: Precipitation characteristics and sensitivities to environmental conditions during

GoAmazon2014/5 and ACRIDICON-CHUVA, Atmos. Chem. Phys., 18, 6461-6482, https://doi.org/10.5194/acp-18-6461-2018

Martin, S. T., Artaxo, P., Machado, L., Manzi, A., Souza, R., Schumacher, C., Wang, J., Andreae, M., Barbosa, H., Fan, J. et al. (2016). Introduction: observations and modeling of the Green Ocean Amazon (GoAmazon2014/5), Atmospheric Chemistry and Physics 16(8): 4785–4797.

Mathon, V. and Laurent, H. (2001). Life cycle of Sahelian mesoscale convective cloud systems, Quarterly Journal of the Royal Meteorological Society 127(572): 377–406.

Matsuno, T. (1966). Quasi-geostrophic motions in the equatorial area, Journal of the Meteorological Society of Japan. Ser. II 44(1): 25–43.

Negri, A. J., Adler, R. F., Nelkin, E. J. and Huffman, G. J. (1994). Regional rainfall climatologies derived from special sensor microwave imager (SSM/I) data, Bulletin of the American Meteorological Society 75(7): 1165–1182.

Nesbitt, S. W., Cifelli, R., and Rutledge, S. A. (2006). Storm morphology and rainfall characteristics of TRMM Precipitation Features. Monthly Weather Review, 134, 2702-2721.

Oliveira A.P., Fitzjarrald D.R. (1993). The Amazon river breeze and the local boundary layer: I - observations. Boundary Layer Meteorology 63:141–162. doi: 10.1007/BF00705380.

Poveda, G., J.C Espinoza, M.D. Zuluaga, S.A. Solman, R. Garreaud, and P.J van Oevelen, (2020). High Impact Weather Events in the Andes. Frontiers in Earth Science, doi: https://doi.org/10.3389/feart.2020.00162.

Rasmussen, K. L., Chaplin, M. M., Zuluaga, M. D., and Houze, R. A. Jr., 2016: Contribution of extreme convective storms to rainfall in South America. J. Hydrometeorol. 17, 353–367. doi: 10.1175/JHM-D-15-0067.1.

Rehbein, A., Ambrizzi, T. and Mechoso, C. R. (2017). Mesoscale convective systems over the Amazon basin. Part I: climatological aspects, International Journal of Climatology.

Rickenbach, T. M. (2004). Nocturnal cloud systems and the diurnal variation of clouds and rainfall in southwestern Amazonia, Monthly Weather Review 132(5): 1201–1219.

Roca, R., Chambon, P., Jobard, I., Kirstetter, P.-E., Gosset, M. and Bergès, J. C. (2010). Comparing satellite and surface rainfall products over West Africa at meteorologically relevant scales during the AMMA campaign using error estimates, Journal of Applied Meteorology and Climatology 49(4): 715–731.

Roca, R., J. Aublanc, P. Chambon, T. Fiolleau, and N. Viltard, 2014: Robust Observational Quantification of the Contribution of Mesoscale Convective Systems to Rainfall in the Tropics. J. Climate, 27, 4952–4958, https://doi.org/10.1175/JCLI-D-13-00628.1.

Santos, M. J., Silva Dias, M. A. F. and Freitas, E. D. (2014). Influence of local circulations on wind, moisture, and precipitation close to Manaus City, Amazon Region, Brazil, Journal of Geophysical Research: Atmospheres 119(23): 13,233–13,249.

Sakamoto, M. S., Ambrizzi, T., and Poveda, G. (2011). Moisture sources and life cycle of convective systems over western Colombia. Advances in Meteorology, vol. 2011, Article ID 890759, 11 pages, https://doi.org/10.1155/2011/890759.

Serra, Y. L., A. Rowe, D. K. Adams, and G. N. Kiladis, 2020: Kelvin Waves during GOAmazon and Their Relationship to Deep Convection. J. Atmos. Sci., 77, 3533–3550, https://doi.org/10.1175/JAS-D-20-0008.1.

Schiro, K. A., J. D. Neelin, D. K. Adams, and B. R. Lintner (2016), Deep convection and column water vapor over tropical land vs. tropical Ocean: A comparison between the Amazon and the tropical Western Pacific, J. Atmos. Sci., 73, 4043–4063, doi:10.1175/JAS-D-16-0119.1.

Silva Dias, M. A. F., et al., (2002). Cloud and rain processes in a biosphere-atmosphere interaction context in the Amazon Region, J. Geophys. Res., 107(D20), 8072, doi:10.1029/2001JD000335.

Sun, W.-Y., and I. Orlanski, 1981: Large mesoscale convection and sea breeze circulation. Part I: Linear stability analysis. J. Atmos. Sci. 38: 1675–1693.

Takayabu, Y. N. (1994). Large-scale cloud disturbances associated with equatorial waves, Journal of the Meteorological Society of Japan. Ser. II 72(3): 433–449.

Tanaka, H. and Ryuguji, O. (1971). Spectrum analysis of tropical cloudiness (I), Journal of the Meteorological Society of Japan. Ser. II 49(1): 13–19.

Tang, S., Xie, S., Zhang, Y., Zhang, M., Schumacher, C., Upton, H., Jensen, M. P., Johnson, K. L., Wang, M., Ahlgrimm, M. et al. (2016). Large-scale vertical velocity, diabatic heating and drying profiles associated with seasonal and diurnal variations of convective systems observed in the GoAmazon2014/5 experiment, Atmospheric Chemistry and Physics 16(22): 14249.

Vila, D. A., Machado, L. A. T., Laurent, H. and Velasco, I. (2008). Forecast and Tracking the Evolution of Cloud Clusters (ForTraCC) using satellite infrared imagery: Methodology and validation, Weather and Forecasting 23(2): 233–245.

Wallace, J. and Chang, L. (1972). On the application of satellite data on cloud brightness to the study of tropical wave disturbances, Journal of the Atmospheric Sciences 29(7): 1400–1403.

Wheeler, M. and Kiladis, G. N. (1999). Convectively coupled equatorial waves: Analysis of clouds and temperature in the wavenumber–frequency domain, Journal of the Atmospheric Sciences 56(3): 374–399.

Williams, M. and Houze Jr, R. A. (1987). Satellite-observed characteristics of winter monsoon cloud clusters, Monthly Weather Review 115(2): 505–519.

Woodley, W. L., Griffith, C. G., Griffin, J. S. and Stromatt, S. C. (1980). The inference of GATE convective rainfall from SMS-1 imagery, Journal of Applied Meteorology 19(4): 388–408.

Zangvil, A. (1975). Temporal and spatial behavior of large-scale disturbances in tropical cloudiness deduced from satellite brightness data, Monthly Weather Review 103(10): 904–920.

Zuluaga, M. D., and R. A. Houze, (2015). Extreme Convection of the Near-Equatorial Americas, Africa, and Adjoining Oceans as seen by TRMM. Mon. Wea. Rev., 143, 298–316, https://doi.org/10.1175/MWR-D-14-00109.1.

Figure Captions

Figure 1. Example of multiple process cloud cluster connection.

Figure 2. AMCS tracking: (a) Initiation at 2014-03-20 00:00, (b) and (c) propagation positions at 2014-03-20 12:00 and 2014-03-21 04:30, respectively and (d) dissipation at 2014-03-21 17:30. The colors describe the infrared brightness temperature and the bi-dimensional trajectory traveled by the systems is shown by the gray contour.

Figure 3. Probability and cumulative distribution functions of the area and lifetime for the 116,701 AMCSs observed during 2014 and 2015.

Figure 4. (a) AMCS density and (b) the TAPEER-BRAIN rain rate average during 2014 and 2015.

Figure 5. AMCS density during 2014 and 2015 for: a) DJF, b) MAM, c) JJA, and d) SON.

Figure 6. Spatial distribution of the AMCS probability of occurrence in five lifetime stages: t_i corresponds to the initiation, t_f to the dissipation and t_1,t_2 and t_3 are intermediary steps in the AMCS lifetime.

Figure 7. Spatial distribution of the initiation of AMCSs with > 4 hour lifecycle that crossed the central Amazon within a 200-km radius around Manaus, which is indicated by the circle.

Figure 8. Probability and cumulative distribution functions of AMCS velocity of propagation and the zonal and meridional components. This type of wind rose shows the AMCS direction of propagation away from the center.

Figure 9. AMCS propagation wind roses every 7°×8° across northern South America. The concentric circles indicate the probability (5%, 10%, and 15%) in each propagation direction and the colors represent the convective system speed classes. Wind speed values between 1 and 21 m/s were binned in 4 m/s and 22.5° of speed and direction, respectively.

Figure 10. TRMM 3B42 Kelvin wave precipitation anomalies for January to March 2014. The Hovmoller encompasses the latitude range nearest Manaus (2.5-3.5° S) from the dateline in the central Pacific to the prime meridian over Africa. The vertical line corresponds to the longitude of Manaus (60°W).

Figure 11. Relationship between area and lifetime of AMCSs in the Amazon region for

positive (red) and negative (blue) Kelvin wave precipitation anomalies during 2014 and 2015.

Figure 12. As in Fig. 9, but only for AMCSs that occur during positive Kelvin wave phases. This type of wind rose shows the AMCS direction of propagation away from the center.

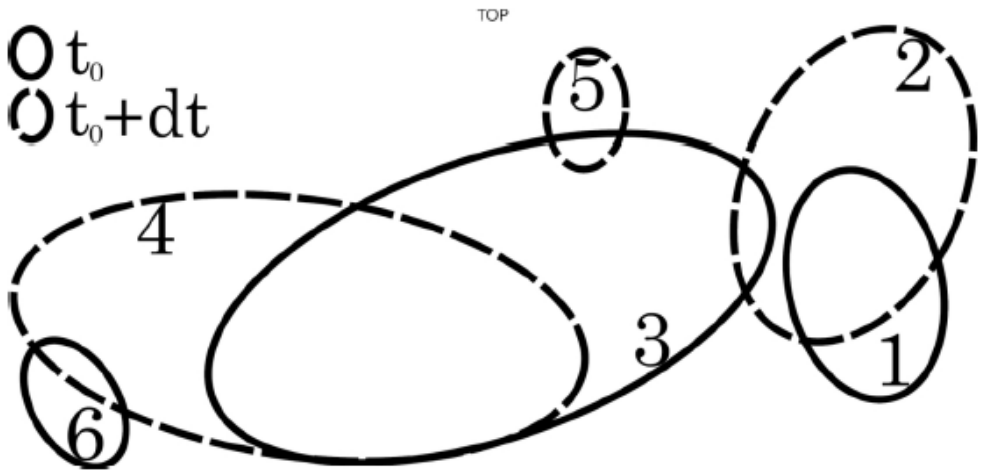

Figure 1. Example of multiple process cloud cluster connection.

127x60mm (300 x 300 DPI)

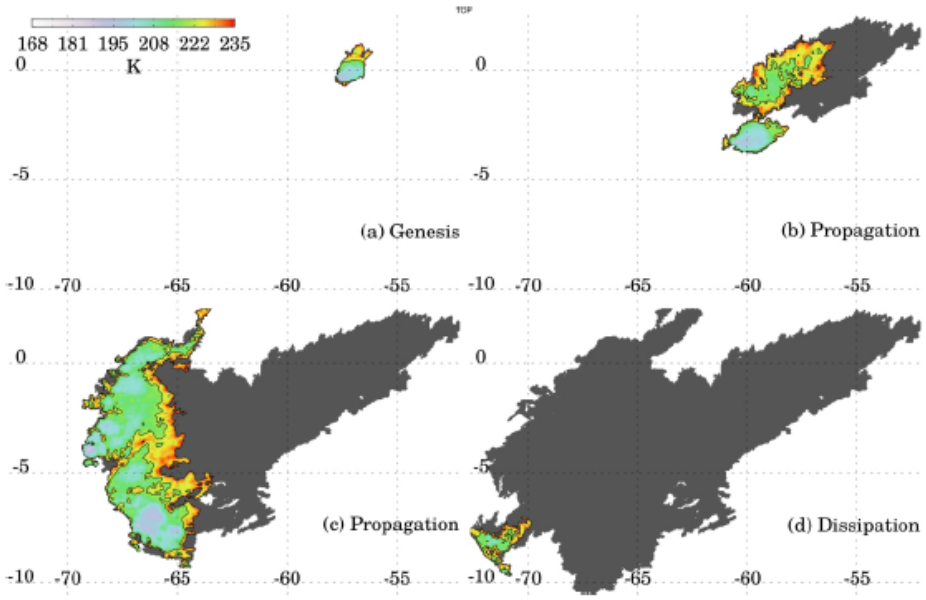

Figure 2. AMCS tracking: (a) Initiation at 2014-03-20 00:00, (b) and (c) propagation positions at 2014-03-20 12:00 and 2014-03-21 04:30, respectively and (d) dissipation at 2014-03-21 17:30. The colors describe the infrared brightness temperature and the bidimensional trajectory traveled by the systems is shown by the gray contour.

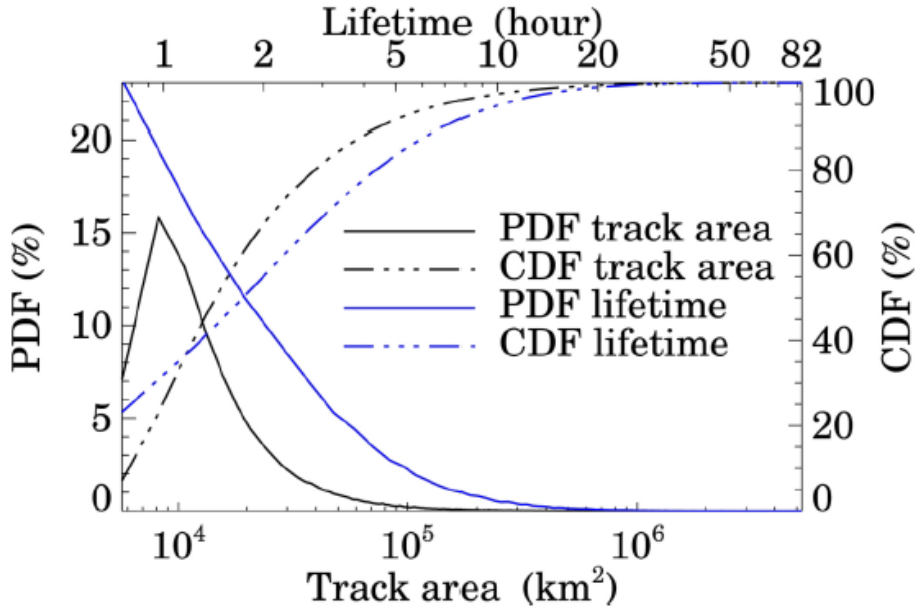

Figure 3. Probability and cumulative distribution functions of the area and lifetime for the 116,701 AMCSs observed during 2014 and 2015.

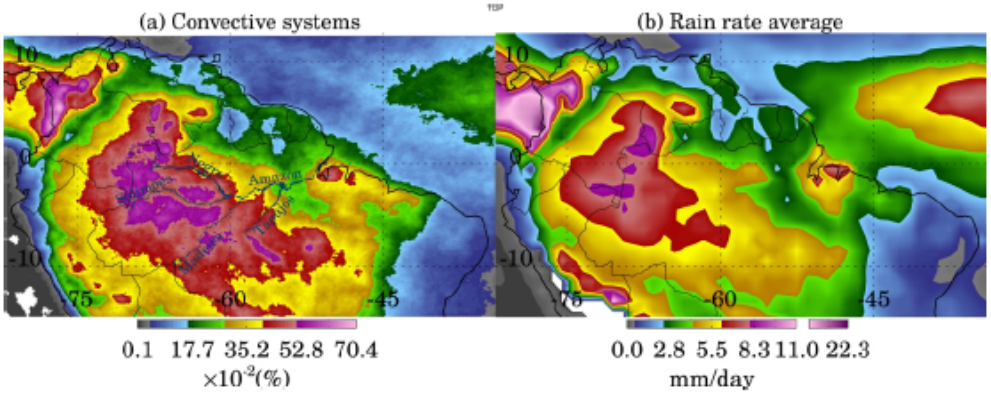

Figure 4. (a) AMCS density and (b) the TAPEER-BRAIN rain rate average during 2014 and 2015.

269x106mm (300 x 300 DPI)

1

2

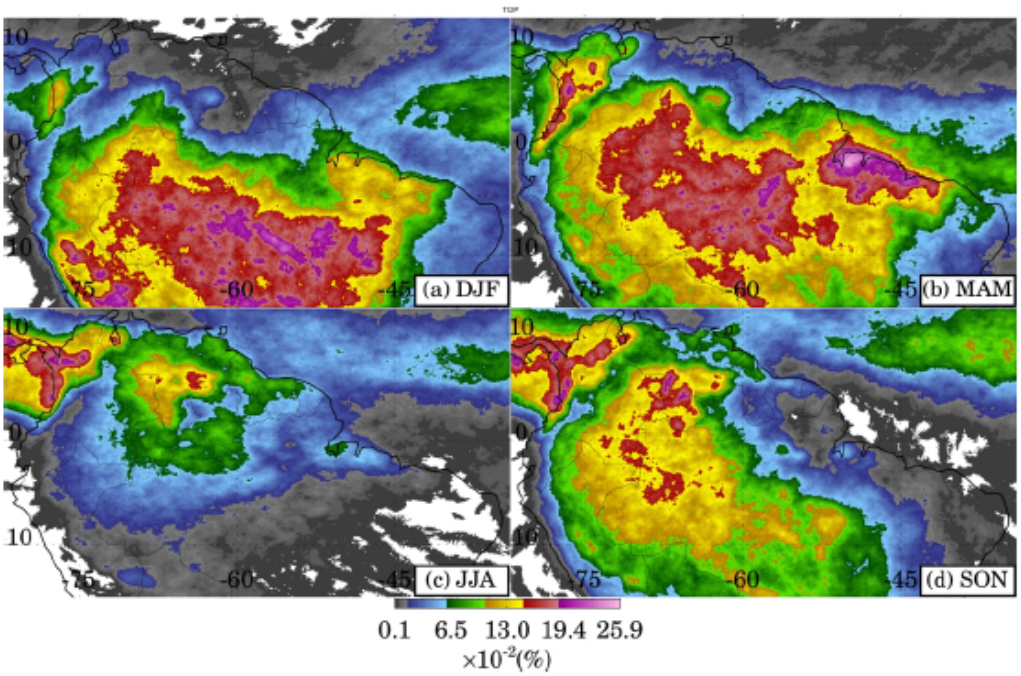

Figure 5. AMCS density during 2014 and 2015 for: a) DJF, b) MAM, c) JJA, and d) SON.

269x177mm (300 x 300 DPI)

3

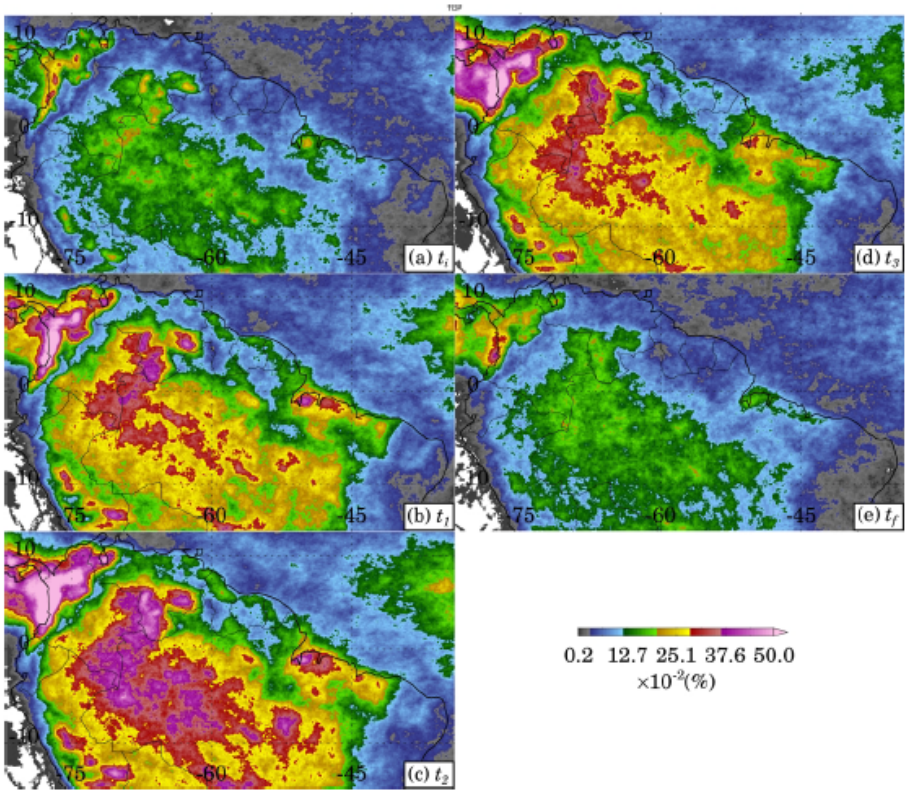

Figure 6. Spatial distribution of the AMCS probability of occurrence in five lifetime stages: t_i corresponds to the initiation, t_f to the dissipation and t_1, t_2 and t_3 are intermediary steps in the AMCS lifetime.

1

2

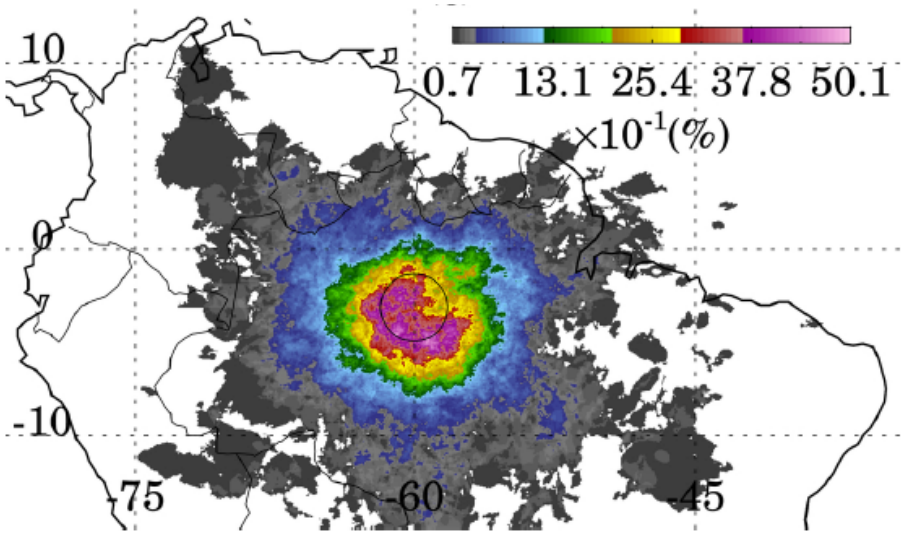

Figure 7. Spatial distribution of the initiation of AMCSs with > 4 hour lifecycle that crossed the central Amazon within a 200-km radius around Manaus, which is indicated by the circle.

3

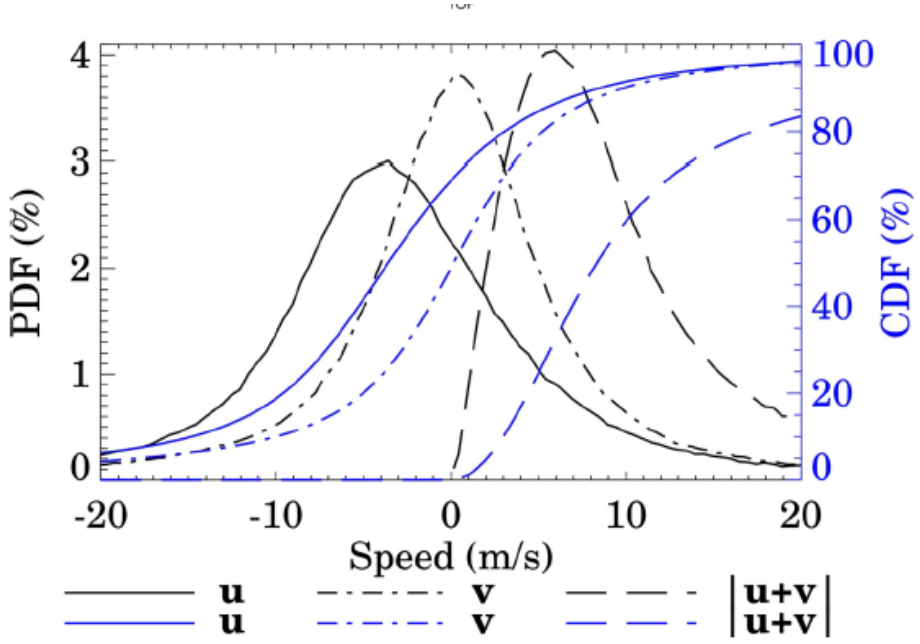

Figure 8. Probability and cumulative distribution functions of AMCS velocity of propagation and the zonal and meridional components.

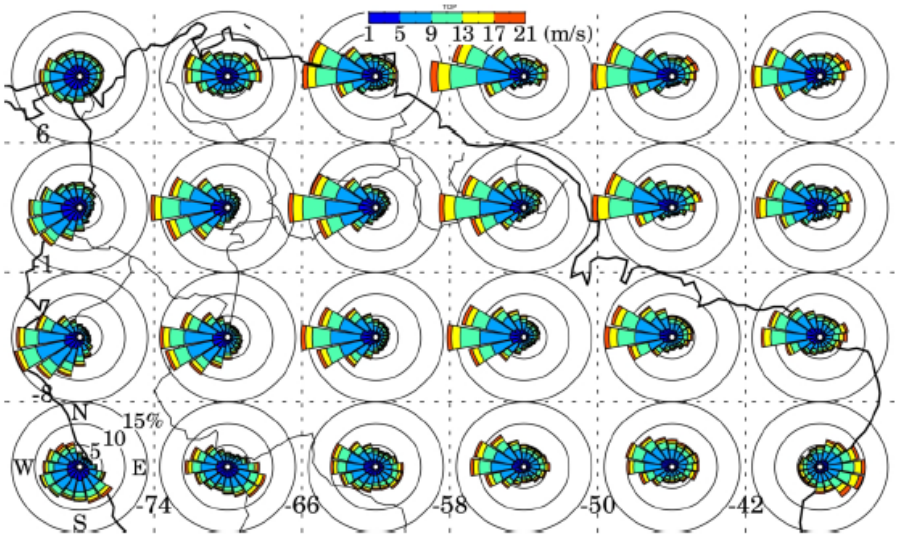

Figure 9. AMCS propagation wind roses every 7°×8° across northern South America. The concentric circles indicate the probability (5%, 10%, and 15%) in each propagation direction and the colors represent the convective system speed classes. Wind speed values between 1 and 21 m/s were binned in 4 m/s and 22.5° of speed and direction, respectively.

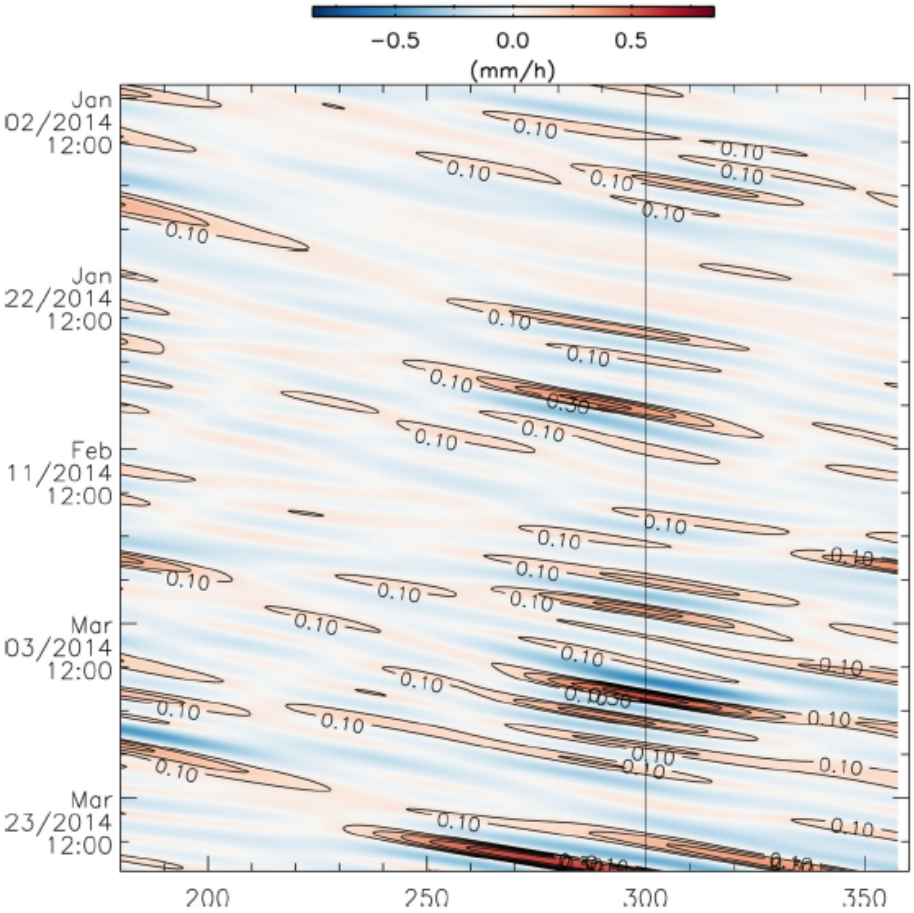

Figure 10. TRMM 3B42 Kelvin wave precipitation anomalies for January to March 2014. The Hovmoller encompasses the latitude range nearest Manaus (2.5-3.5° S) from the dateline in the central Pacific to the prime meridian over Africa. The vertical line corresponds to the longitude of Manaus (60°W).

1

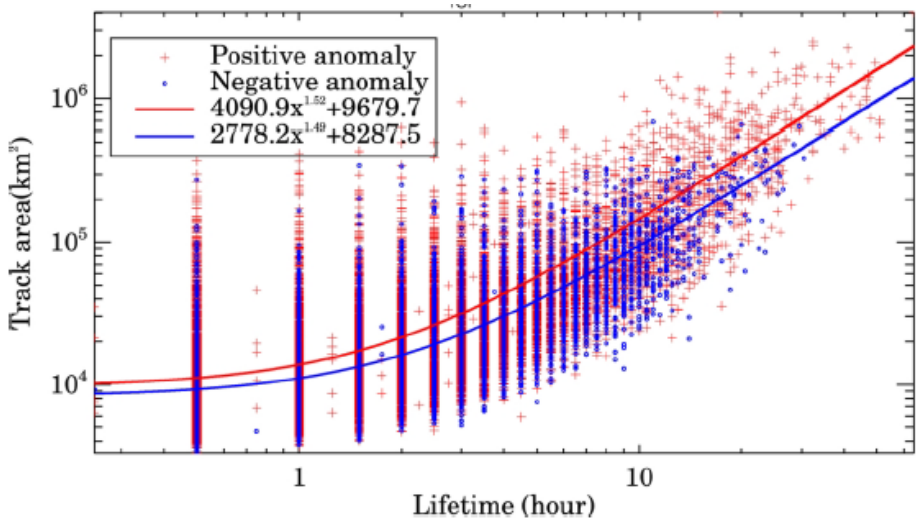

Figure 11. Relationship between area and lifetime of AMCSs in the Amazon region for positive (red) and negative (blue) Kelvin wave precipitation anomalies during 2014 and 2015.

2

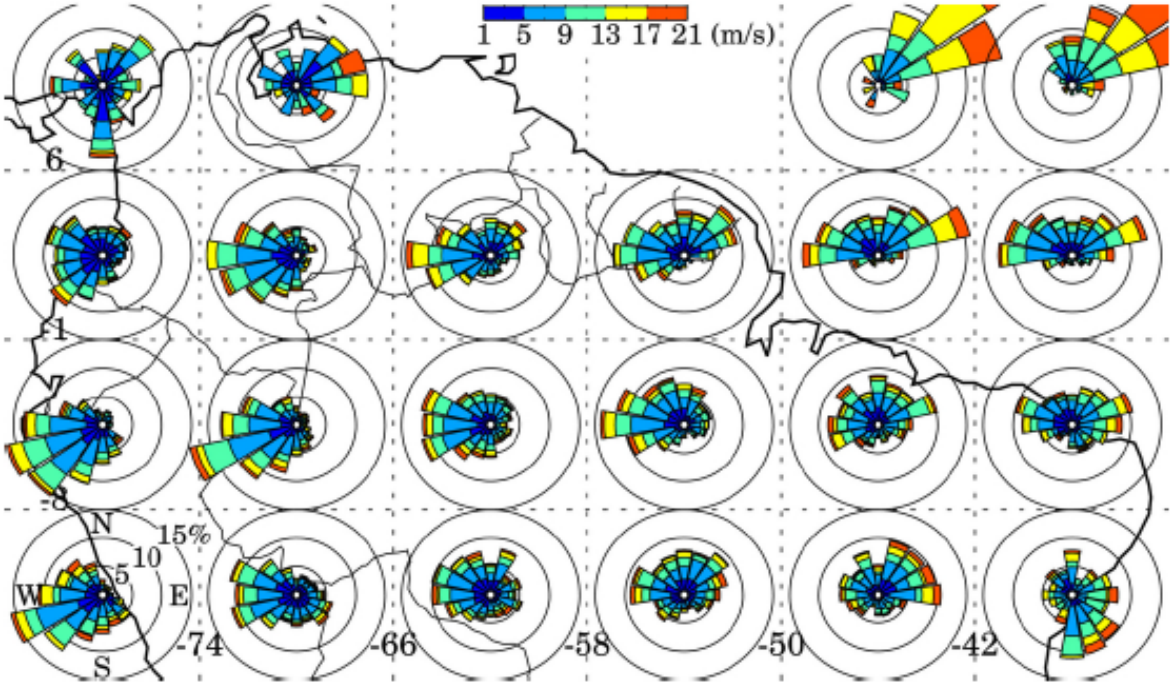

Figure 12. As in Fig. 9, but only for AMCSs that occur during positive Kelvin wave phases.

1